Loss in long-storage-time optical cavities

T. Isogai, J. Miller, P. Kwee, L. Barsotti and M. Evans

LIGO Laboratory, Massachusetts Institute of Technology,
Cambridge, MA, 02139
jmiller@ligo.mit.edu

Abstract: Long-storage-time Fabry-Perot cavities are a core component of many precision measurement experiments. Optical loss in such cavities is a critical parameter in determining their performance; however, it is very difficult to determine a priori from independent characterisation of the individual cavity mirrors. Here, we summarise three techniques for directly measuring this loss in situ and apply them to a high-finesse, near-concentric, 2 m system. Through small modifications of the cavity's length, we explore optical loss as a function of beam spot size over the 1-3 mm range. In this regime we find that optical loss is relatively constant at around 5 ppm per mirror and shows greater dependence on the positions of the beam spots on the cavity optics than on their size. These results have immediate consequences for the application of squeezed light to advanced gravitational-wave interferometers.

OCIS codes: (120.2230) Fabry-Perot; (290.0290) Scattering; (120.3180) Interferometry.

References and links

1. N. Hinkley, J. A. Sherman, N. B. Phillips, M. Schioppo, N. D. Lemke, K. Beloy, M. Pizzocaro, C. W. Oates, and A. D. Ludlow, "An Atomic Clock with 10^{-18} Instability," Science **341**, 1215–1218 (2013).
2. T. Kessler, C. Hagemann, C. Grebing, T. Legero, U. Sterr, F. Riehle, M. J. Martin, L. Chen, and J. Ye, "A sub-40-mHz-linewidth laser based on a silicon single-crystal optical cavity," Nature Photonics **6**, 687–692 (2012).
3. B. Willke et al., "The GEO-HF project," Classical and Quantum Gravity **23**, 207 (2006).
4. G. M. Harry and the LIGO Scientific Collaboration, "Advanced LIGO: the next generation of gravitational wave detectors," Classical and Quantum Gravity **27**, 084006 (2010).
5. The Virgo Collaboration, "Advanced Virgo Baseline Design," Tech. Rep. VIR-0027A-09, https://tds.ego-gw.it/ql/?c=6589 (2009).
6. F. Della Valle, U. Gastaldi, G. Messineo, E. Milotti, R. Pengo, L. Piemontese, G. Ruoso, and G. Zavattini, "Measurements of vacuum magnetic birefringence using permanent dipole magnets: the PVLAS experiment," New Journal of Physics **15**, 053026 (2013).
7. C. J. Hogan, "Interferometers as probes of Planckian quantum geometry," Phys. Rev. D **85**, 064007 (2012).
8. B. P. Abbott et al., "Observation of a kilogram-scale oscillator near its quantum ground state," New Journal of Physics **11**, 073032 (2009).
9. H. J. Kimble, Y. Levin, A. B. Matsko, K. S. Thorne, and S. P. Vyatchanin, "Conversion of conventional gravitational-wave interferometers into quantum nondemolition interferometers by modifying their input and/or output optics," Phys. Rev. D **65**, 022002 (2002).
10. J. Vinet, P. Hello, C. N. Man, and A. Brillet, "A high accuracy method for the simulation of non-ideal optical cavities," Journal de Physique I **2**, 1287–1303 (1992).
11. M. Evans, L. Barsotti, P. Kwee, J. Harms, and H. Miao, "Realistic filter cavities for advanced gravitational wave detectors," Phys. Rev. D **88**, 022002 (2013).
12. A. E. Siegman, *Lasers* (University Science Books, 1986).
13. M. J. Lawrence, B. Willke, M. E. Husman, E. K. Gustafson, and R. L. Byer, "Dynamic response of a Fabry-Perot interferometer," Journal of the Optical Society of America B Optical Physics **16**, 523–532 (1999).
14. M. Rakhmanov, "Doppler-Induced Dynamics of Fields in Fabry-Perot Cavities with Suspended Mirrors," Appl. Opt. **40**, 1942–1949 (2001).

15. L. Zhang, G. Billingsley, and M. Phelps, "QA Test Procedure for aLIGO COC," LIGO Technical Report E1000863-v2 (2011).
16. D. Jacob, M. Vallet, F. Bretenaker, A. Le Floch, and M. Oger, "Supermirror phase anisotropy measurement," Optics Letters **20**, 671–673 (1995).
17. F. Magaña-Sandoval, R. X. Adhikari, V. Frolov, J. Harms, J. Lee, S. Sankar, P. R. Saulson, and J. R. Smith, "Large-angle scattered light measurements for quantum-noise filter cavity design studies," Journal of the Optical Society of America A **29**, 1722 (2012).
18. F. Magaña-Sandoval, J. R. Smith et al., "A comparison of optical scatter from coated and uncoated optics for quantum noise filter cavities," In Preparation (2013).
19. C. C. Gerry, *Introductory quantum optics* (Cambridge University Press, Cambridge, UK New York, 2005).
20. J. Abadie et al., "A gravitational wave observatory operating beyond the quantum shot-noise limit," Nature Physics **7**, 962–965 (2011).
21. J. Aasi et al., "Enhanced sensitivity of the LIGO gravitational wave detector by using squeezed states of light," Nature Photonics **7**, 613–619 (2013).

1. Introduction

Long-storage-time optical cavities are an essential tool in the quest to expand our understanding of the universe. Currently, these devices are employed in the world's best clocks [1] and frequency references [2]; experiments exploring strong-field General Relativity, the structure of nuclear matter and the validity of cosmological models [3, 4, 5]; searches for vacuum birefringence [6] and holographic noise [7]; and studies of macroscopic quantum mechanics [8] and the squeezed-state rotation produced by filter cavities [9].

The storage time of an optical cavity is defined as the time taken for the cavity field to decay by $1/e$. For a cavity of length $\mathscr{L}_{\text{cavity}}$ and finesse $\mathscr{F}$ (see (6)), the storage time can be written as

$$\tau_{\text{storage}} = \frac{2\mathscr{L}_{\text{cavity}}\mathscr{F}}{\pi c} = \frac{\mathscr{F}}{\pi f_{\text{FSR}}}, \tag{1}$$

where $f_{\text{FSR}} = c/(2\mathscr{L}_{\text{cavity}})$ is the cavity free-spectral-range. The storage time is therefore directly proportional to the product of finesse and cavity length. Optical loss, predominantly due to scattering from the surfaces of the cavity optics, limits the achievable finesse and storage time for a given cavity length.

Although the surfaces of mirrors can be mapped with nm-level precision and the absorption of bulk materials is well-known, a number of effects prevent an accurate extrapolation from these measurements to the optical loss which will be observed when a cavity is formed. Dependence on spot position, coating defects, the capture of higher-order modes and other unexplained mechanisms all conspire to make theoretical analyses intractable. Simulations are equally challenging, even when performed using FFT-based techniques [10].

Previous measurements of loss in long-storage time cavities were made on a variety of disparate systems during the course of other investigations. These results suggest that optical loss increases with beam spot size, implying that an almost confocal cavity is optimal (since this geometry has the smallest beam spots for a given cavity length). The following expression is an empirical scaling law based on the data reported in Figure 4 of [11],

$$L_{\text{rt}}(\mathscr{L}_{\text{confocal}}) = 10\ \text{ppm} \cdot \left(\frac{\mathscr{L}_{\text{confocal}}}{1\ \text{m}}\right)^{0.3}. \tag{2}$$

Here L_{rt} is the round-trip loss and $\mathscr{L}_{\text{confocal}}$ is the length of the confocal cavity which has the same spot size at its mirrors as the cavity whose losses were published (see (7)).

This approximation of the experimental results, was not based on any physical analysis and has never been verified under controlled conditions using coherent methods. In this work, to the best of our knowledge, we present the first systematic study of optical loss in a long-storage-time cavity as a function of beam spot size.

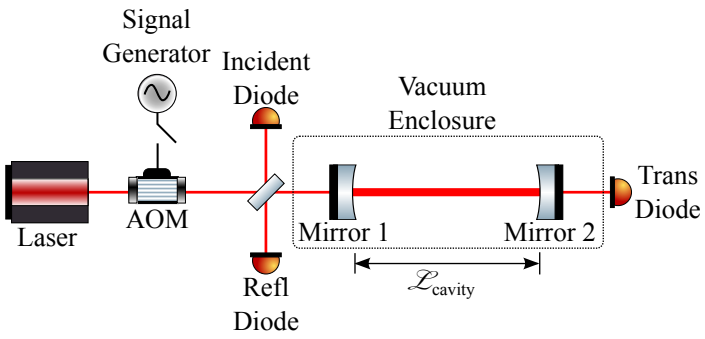

Fig. 1. A schematic representation of our experimental apparatus. See §3 for additional detail.

2. Definition of cavity loss

The optical properties of a mirror may be characterised by conservation of energy,

$$R+T+L=R+A=1, \tag{3}$$

where $R=r^2$ is the power reflectivity, $T=t^2$ is the power transmissivity and L is the coefficient of power loss. We also introduce the attenuation, $A=T+L$, to describe the total power lost *from the cavity* upon a single reflection.

Our goal is to investigate the round-trip loss of a two-mirror cavity, $L_{\text{rt}}=L_1+L_2$. Here and henceforth subscript 1 refers to the cavity input mirror and subscript 2 to the cavity end mirror (see Fig. 1).

A quantity which is easily accessible via experiment is the round-trip (amplitude) reflectivity, $r_1 r_2$. Beginning from (3) and expanding $r_1 r_2$ to first order in L and T, the round-trip loss may be cast in the form

$$L_{\text{rt}}=2(1-r_1 r_2)-(T_1+T_2). \tag{4}$$

Whence we also define the round-trip attenuation

$$A_{\text{rt}}=A_1+A_2=2(1-r_1 r_2). \tag{5}$$

In practice, we are able to measure the round-trip attenuation A_{rt} and the input mirror transmissivity T_1, which, for our strongly overcoupled cavity, are the only relevant parameters. Therefore, we simplify our analysis by setting $r_2=1$ ($T_2=0$), effectively incorporating the transmissivity and loss of the end mirror into the loss of the input mirror such that A_{rt}=T_1+L_1.

3. Description of the experimental set-up

A symmetric, near-concentric ($\text{ROC}_1=\text{ROC}_2\simeq\mathscr{L}_{\text{cavity}}/2$) optical cavity of length $\mathscr{L}_{\text{cavity}}\lesssim 2$ m was chosen for our study. This geometry allowed the spot size on the cavity optics to be varied over a wide range via small ($\sim$1 cm) changes in cavity length.

To mitigate environmental disturbances and prevent contamination, the system was housed in a vacuum enclosure operating below 10^{-4} mbar and mounted on an optical table equipped with pneumatically isolating legs (Newport S-2000 series). The level of ambient particulates was controlled by conducting the experiment within a class 100 soft-wall clean room. Appropriate dress and housekeeping standards were strictly observed.

The cavity optics consisted of ion-beam-sputtered coatings deposited atop super-polished, two-inch, fused-silica substrates (RMS roughness $<$1 Å, 10-5 scratch-dig surface quality). The

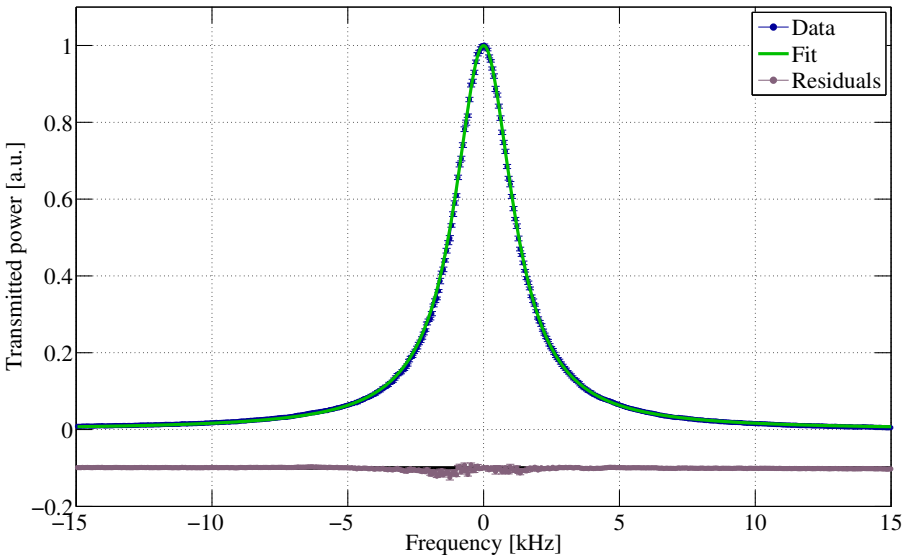

Fig. 2. A representative linewidth measurement. 30,000 samples were taken at each of 500 frequencies over a 30 kHz span. Residuals are offset by -0.1 for clarity.

methods used in the manufacture of these optics represent the current state of the art. The measured transmissivities at our measurement wavelength were 192.2±1.3 ppm for Mirror 1 and 1.55±0.14 ppm for Mirror 2 (see Fig. 1); yielding a finesse of ∼30,000 and a linewidth of ∼2.5 kHz. The optics were held in custom Siskiyou IXM200 mounts which were actuated upon by New Focus 8301-UHV picomotors. Prior to use, the cavity mirrors were thoroughly cleaned using spectral-grade solvents.

The cavity input beam was generated by a 1064 nm diode-pumped solid-state laser (JDSU M126N-1064-500). Before injection into the cavity, the input beam was double-passed through an acousto-optic modulator (AOM). The AOM (Gooch and Housego 3200-1113) was operated over a 100 MHz band about its centre frequency of 200 MHz. By modifying the frequency of the AOM drive signal, the detuning of the input beam from resonance could be accurately controlled. Moreover, by interrupting the AOM drive, the cavity input light could be extinguished on a timescale of ∼10 ns. The power at the output of the AOM was ∼1 mW.

In order to suppress cavity length noise and laser frequency fluctuations, a frequency-shifted sample of the cavity input beam, picked off prior to the AOM, was locked to the cavity at all times by actuating on the laser's frequency (∼40 kHz bandwidth). This arrangement is not shown in Fig. 1.

Readout was effected by three high-bandwidth photodetectors. Two to sample the light transmitted and reflected by the cavity (Trans Diode and Refl Diode respectively) and a third (Incident Diode) to compensate for variations in laser power and the frequency dependence of AOM output power.

4. Measurement techniques

We now describe the three methods used to determine the optical loss of our cavity. Each of the techniques is able to measure round-trip attenuation whilst the third also yields input mirror transmissivity, allowing round-trip loss to be extracted.

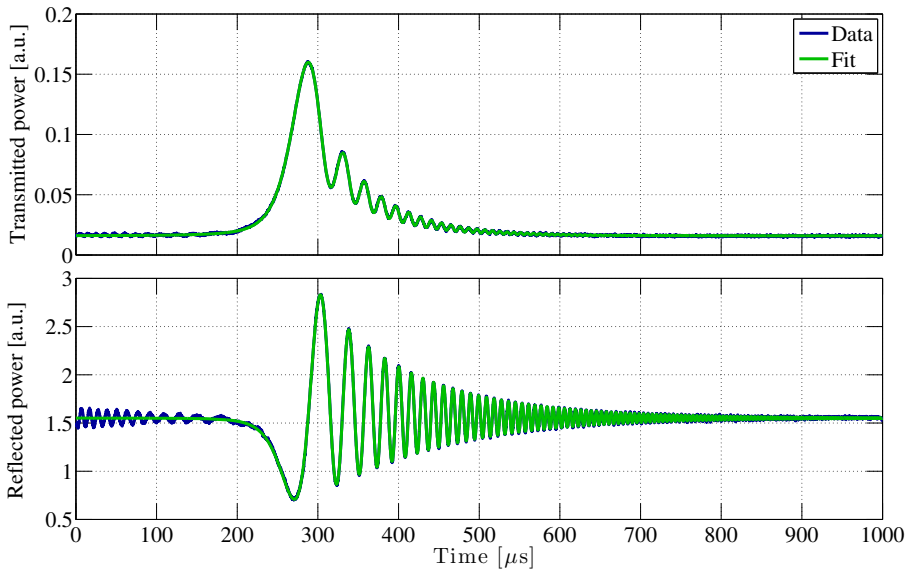

Fig. 3. Typical Doppler measurement. Deviations of the fit function (green) from recorded data (blue) at early times are explained by start-up transients (cavity field decaying to a steady state after light is injected) which are present in experiment but were not included in our theoretical model. This effect has no influence on the extracted fit parameters.

All three techniques require knowledge of the cavity free-spectral-range, f_{FSR}. This quantity was measured to an uncertainty of $\sim$100 Hz by noting the change in AOM drive frequency required to move between adjacent longitudinal modes of the cavity.

The cavity g-factor [12] was evaluated in a similar fashion by using the AOM to map out the resonant frequencies of higher-order spatial modes. From this description of the cavity geometry one can calculate informative parameters such as cavity waist size, beam spot size on the cavity mirrors and equivalent confocal cavity length [12].

4.1. *Cavity linewidth*

A straightforward evaluation of the cavity full-width-half-maximum-power linewidth, f_{FWHM}, was made by recording the power transmitted by the cavity as the AOM slowly stepped the input laser frequency across a fundamental-mode resonance and fitting the result (see Fig. 2). With this information and knowledge of f_{FSR} one can readily calculate the finesse,

$$\mathscr{F} = \frac{f_{\mathrm{FSR}}}{f_{\mathrm{FWHM}}} = \frac{\pi\sqrt{r_1 r_2}}{1 - r_1 r_2}, \tag{6}$$

and therefore the round-trip attenuation (see (5)).

4.2. *Doppler*

A second, similar, method also involved tuning the laser frequency across resonance; however, in this instance, the laser frequency was made to sweep linearly through resonance on a timescale comparable to the cavity storage time τ_{storage} ($\sim$100 µs for our system, see (1)).

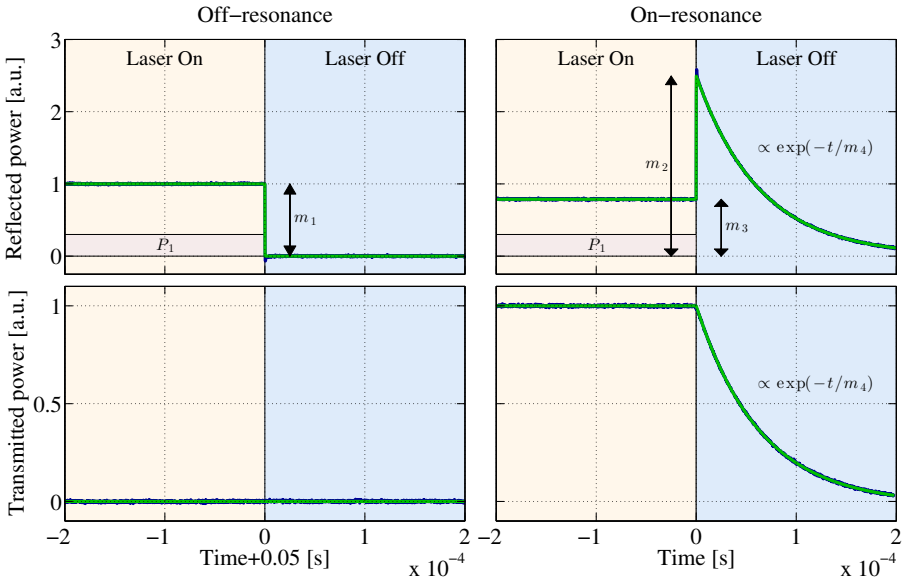

Fig. 4. Illustrative ringdown measurement showing reflected (upper axes) and transmitted (lower axes) powers. Data are shown in blue and theoretical fits in green. Deviations between the curves around $t = 0$ are due to the finite detection bandwidth. A visually imperceptible downsampling factor of twenty five has been applied to the plotted data.

In this case, previously studied dynamical effects are observed (see e.g. [13, 14]), with both the transmitted and reflected powers exhibiting damped oscillations (see Fig. 3). The decay time of these oscillations is given by τ_{storage}, from which we again determine the cavity finesse and round-trip attenuation.

4.3. Ringdown

The final technique employed capitalises on our ability to quickly extinguish the cavity input light. Beginning from a steady-state resonant condition, the drive to the AOM is interrupted, cutting the input light and causing the power stored in the cavity to decay. If one describes the cavity input power as $P_{\text{in}} = P_0 + P_1$, where P_0 (P_1) is that portion coupled (not coupled) into the fundamental cavity mode, then the power circulating in the cavity n round-trips after the input light is extinguished (at $t = 0$) is given by

$$P_{\text{cav}}(n) = P_0 G T_1 (R_1 R_2)^n,$$

where $G = g^2 = [1/(1 - r_1 r_2)]^2$ is the cavity gain, or, extrapolating to a function of continuous time,

$$P_{\text{cav}}(t \geq 0) = P_0 G T_1 (R_1 R_2)^{t/\tau_{\text{rt}}} = P_0 G T_1 \exp(-2t/\tau_{\text{storage}})$$

where $\tau_{\text{rt}} = 1/f_{\text{FSR}} = 2\mathscr{L}_{\text{cavity}}/c$ is the cavity round-trip time and τ_{storage} may alternatively be written

$$\tau_{\text{storage}} = -\frac{1}{f_{\text{FSR}} \log(r_1 r_2)} \simeq \frac{g}{f_{\text{FSR}}}.$$

Therefore the transmitted and reflected powers are given by

$$P_{\text{trans}}(t) = \begin{cases} P_0 G T_1 T_2 & \text{t<0,} \\ P_0 G T_1 T_2 \exp(-2t/\tau_{\text{storage}}) & \text{t}\geq 0 \end{cases}$$

and

$$P_{\text{refl}}(t) = \begin{cases} P_0 G[r_1 - r_2(T_1 + R_1)]^2 + P_1 & \text{t}<0, \\ P_0 G T_1^2 R_2 \exp(-2t/\tau_{\text{storage}}) & \text{t}\geq 0, \end{cases}$$

where, in both cases, the expressions for $t < 0$ are those of the standard steady state [12].

In both transmission and reflection one can easily fit the decaying portion of these waveforms to extract τ_{storage} and therefore quantify the round-trip attenuation – a traditional ringdown measurement. However, in reflection additional information is available which makes it possible to also extract input mirror transmissivity.

Experimentally, two synchronised square-wave modulations were applied to the AOM drive such that the laser input light was 1) switched on and off at a frequency $f_{\text{mod}} = 40$ Hz and 2) made to alternate between resonant and off-resonance tunings at a frequency of $f_{\text{mod}}/2$. In combination, these modulations allowed us to record the diode outputs as the cavity transitioned between four states: off-resonance laser-on, off-resonance laser-off, on-resonance laser-on and on-resonance laser-off. From these data we extracted photodetector offsets and the four quantities indicated in Fig. 4,

$$\begin{aligned} m_1 &= P_0 + P_1, \\ m_2 &= P_0 G T_1^2 R_2, \\ m_3 &= P_0 G[r_1 - r_2(T_1 + R_1)]^2 + P_1, \\ m_4 &= \tau_{\text{storage}}/2. \end{aligned}$$

These measurements define four equations in five variables (P_0, P_1, r_1, t_1 and r_2). In order to compute a solution we again choose to set $r_2 = 1$ (see §2)[1].

From this solution we can construct not only the round-trip attenuation, as before, but also the round-trip loss, $L_{\text{rt}} = A_{\text{rt}} - t_1^2$, and the input mode-matching fraction, $P_0/(P_0 + P_1)$. Moreover, the t_1 value obtained in this way can also be used to convert round-trip attenuation values obtained via other measurement techniques into round-trip loss.

On average, this method of obtaining t_1 was found to give results consistent with independent transmissivity measurements [15]. However, the ringdown-based technique is preferred as it probes the same region of each mirror's surface as the attenuation measurement, accounting for any spatial variation in transmissivity even as the cavity axis moves. In contrast, the two-dimensional transmissivity map of a witness sample, or even an installed optic, can produce only an informed estimate for use in analysis.

5. Results

The length of our cavity was varied from 1.932 m to 1.998 m in four discrete steps. This range of lengths provided beam spot sizes extending from 1.34 mm to 2.74 mm. Examination of larger spot sizes was prohibited by cavity instability.

At every cavity length, several different alignments were investigated. Each alignment resulted in a new cavity axis, displaced by approximately one beam spot size at both mirrors. Explorations of larger axis shifts produced no appreciable difference in recorded results.

This combination of length and alignment changes allowed us to investigate optical loss as a function of beam spot size in a systematic way, accounting for the possible influence of coating inhomogeneities and defects.

For every configuration, the techniques detailed in §4 were each applied one hundred times, mitigating the effects of random noise and enabling drifts to be investigated and eliminated.

[1] For cavities with matched coatings one can take $r_1 = r_2$. Alternatively, performing a second set of measurements after swapping Mirror 1 and Mirror 2 allows one to immediately solve the system.

5.1. *Attenuation measured by each technique*

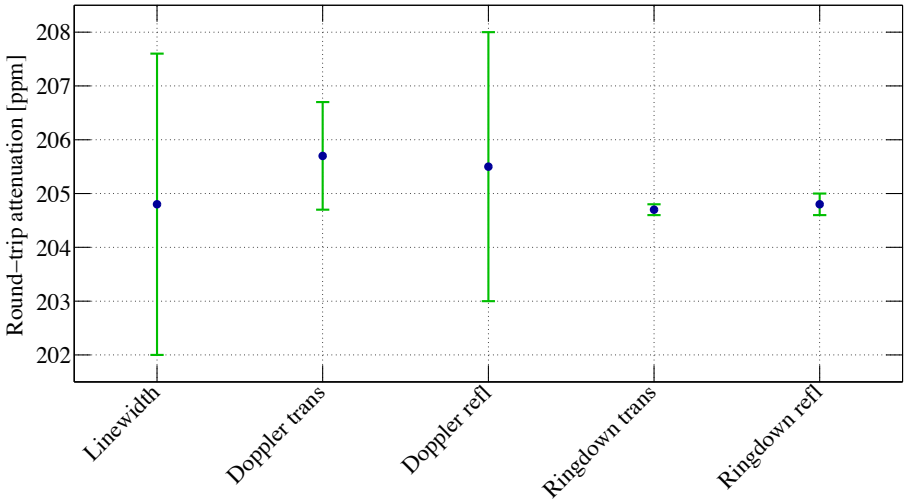

Fig. 5. Round-trip attenuation measured using five techniques at a single cavity length and alignment. Uncertainties represent the statistical error of one hundred measurements.

Typical results for a single measurement configuration are shown in Fig. 5. The mean round-trip attenuation values from all techniques agree to better than 1 ppm. This uniformity was preserved at all alignments and cavity lengths, engendering confidence in our experimental method and analysis pipelines.

Achieving such consistency demanded the painstaking examination and elimination of experimental noise sources (particularly troublesome were scattered light and indiscernible beam clipping) and systematic effects (cavity-induced polarisation rotation [16], electronic offsets and pressure and temperature changes in the vacuum vessel).

The relative magnitudes of the uncertainties may be explained by the timescale over which the experimental data were captured. Linewidth measurements were made comparatively slowly and were therefore more susceptible to any unintended detunings from resonance. In our set-up, such detunings were mainly due to residual seismic and acoustic disturbances. Doppler and ringdown measurements were performed much more quickly and were hence less sensitive to low-frequency environmental noise, resulting in smaller variations within a measurement set.

In addition to being performed most quickly, the small uncertainties offered by ringdown measurements may further be ascribed to the non-resonant nature of the technique – after input light has been extinguished, cavity length fluctuations are no longer able to influence ringdown results.

5.2. *Attenuation and transmissivity as function of beam spot position*

In Fig. 6 we show how the outcome of one measurement technique (ringdown in reflection) varied as a function of alignment at a single cavity length. We observe that the round-trip attenuation undergoes changes more than one order of magnitude larger than its experimental uncertainty whilst the simultaneously measured input mirror transmissivity remains relatively constant. Equivalent behaviour was witnessed in all of our data. Thus, beam spot position had a strong influence on round-trip optical loss. Independent measurements of scatter and absorption as a function of beam position were not available to correlate against our measured data.

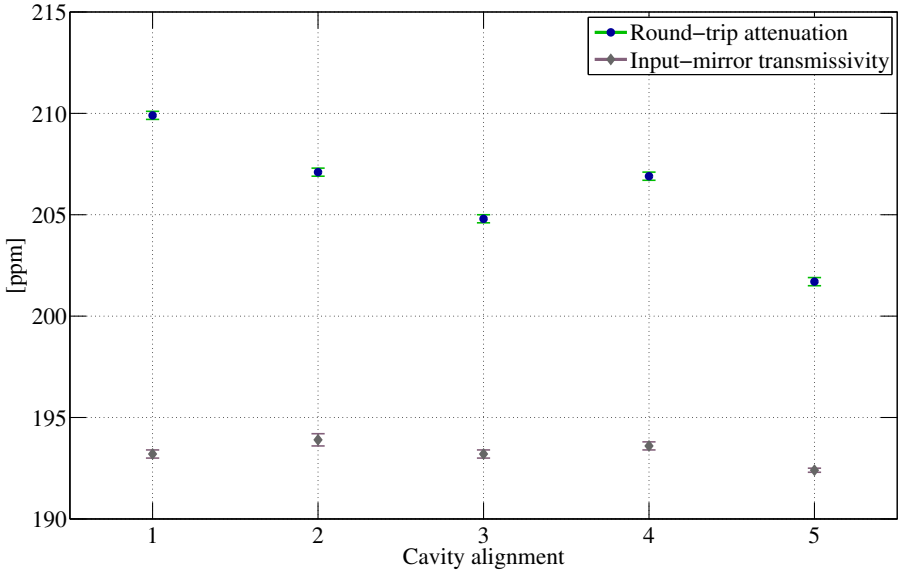

Fig. 6. Round-trip attenuation and input-mirror transmissivity obtained via ringdown measurements in reflection at five different cavity alignments. Uncertainties represent the statistical error of one hundred measurements.

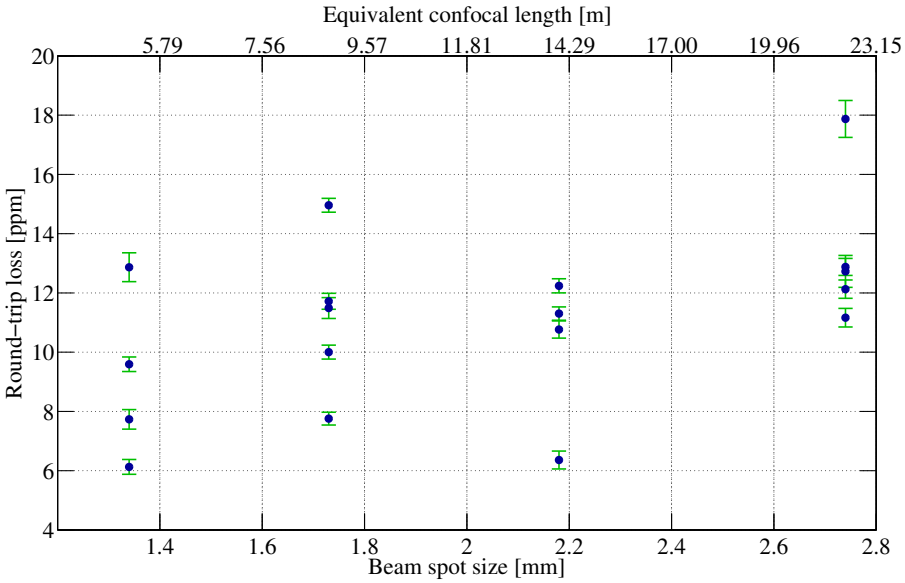

Fig. 7. Measured round-trip loss as a function of beam spot size and equivalent confocal length. Each data point corresponds to the combined outcome (weighted by statistical uncertainty) of three different measurement techniques applied at a single cavity length and alignment. The resulting experimental error is almost equally distributed between uncertainty in determination of T_1, T_2 and A_{rt}. Several alignments were explored at each cavity length, yielding multiple loss values for each beam spot size. Equivalent confocal lengths are rounded to two decimal places.

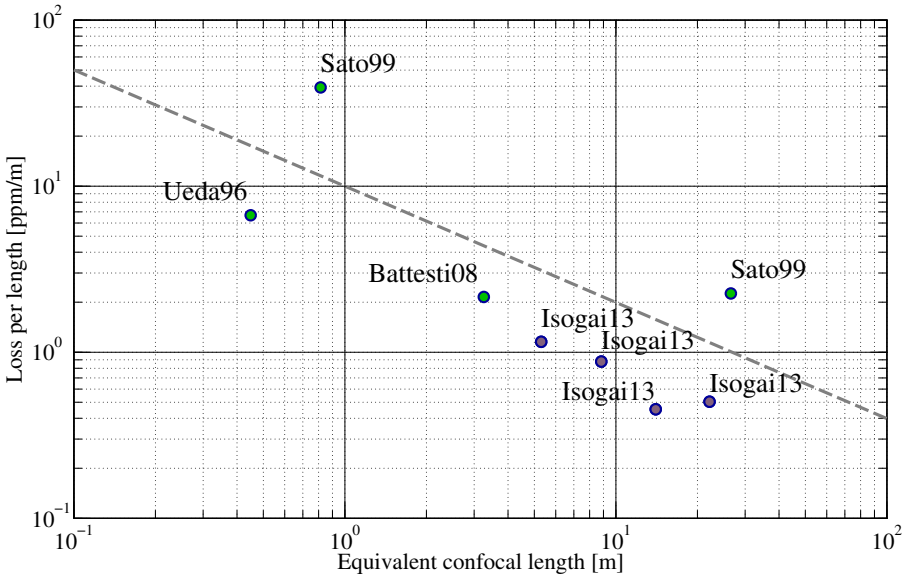

Fig. 8. Loss per unit length as a function of equivalent confocal length. Our results (Isogai13, blue and violet markers) are compared to previously published works. References are available in Figure 4 of [11], from where this plot was reproduced with permission.

5.3. Round-trip loss as function of beam spot size and equivalent confocal length

Results from all measurement techniques, cavity lengths and spot positions are combined in Fig. 7 to show round-trip optical loss as a function of beam spot size.

In addition to utilising all information available from experiment, we also subtract the value of T_2 (1.55±0.14 ppm), obtained via independent examination of a coating witness sample [15], from our estimate of L_{rt}. T_2 cannot be directly measured in our set-up but tacitly contributes to the round-trip attenuation A_{rt} as we chose to set $r_2 = 1$.

In Fig. 7 we also characterise our results in terms of the equivalent confocal cavity length

$$\mathscr{L}_{\mathrm{confocal}} = \frac{\pi w^2}{\lambda_{\mathrm{laser}}}, \tag{7}$$

where w is the beam spot size on the cavity optics and λ_{laser} is the wavelength of the input laser light. For a given spot size, a confocal geometry gives the longest possible cavity and therefore the narrowest linewidth, the longest storage time and the best frequency or length discrimination. Numerical simulations of ten concentric cavities and their confocal equivalents, with spot sizes ranging from 1.2 mm to 3.9 mm and realistically imperfect optics, revealed no significant geometry-dependent variations in loss.

It should be noted that, due to alignment sensitivity, data taken when the beam spot size was at its largest (2.74 mm) were not of a quality equivalent to the remainder of the data. Whilst the values presented are an accurate representation of the measured loss when the cavity alignment was optimal, small perturbations resulted in values larger by tens of ppm, presumably due to beam clipping. For the same reason, linewidth measurements proved unreliable for the largest spot size and were not incorporated into our analysis.

To set our results in context, we plot our lowest-loss results for each cavity length together with values obtained from the literature (see Fig. 8). Data are described in terms of loss per unit length, where, for the reasons discussed above, the length is that of the equivalent confocal cavity.

6. Discussion and conclusions

In this work we have performed the first, to our knowledge, systematic investigation of optical loss as a function of beam spot size. We find that our cavity mirrors, representative of the best available at this time, offer an approximately constant round-trip optical loss of $\sim$10 ppm (5 ppm per bounce) for beam spot sizes in the 1-3 mm range (equivalently, confocal lengths in the 5-25 m range). It is important to note, however, that a significant range of optical losses ($\sim$6 ppm to $\sim$18 ppm) was observed as the position of the beam spots on the cavity mirrors was varied.

From our measurements we conclude that variations in loss result from scattering caused by point defects with an average separation larger than a few millimetres. This conclusion is supported by direct measurements of the scattering produced by our cavity mirrors, made following the methods described in [17]. The total integrated scatter of each of our optics (measured using a 4-6 mm beam spot) was estimated to be $\sim$10 ppm [18], comparable to the per-bounce loss inferred from the data presented in Fig. 7.

The results presented here are of immediate interest in relation to ground-based interferometric gravitational-wave detectors (e.g. Advanced LIGO [4]). Squeezed states of light [19] have recently been shown to enhance the sensitivity of gravitational-wave interferometers by reducing quantum shot noise at high frequencies ($\gtrsim$100 Hz) [20, 21]. Future interferometers require that the squeezed quadrature be rotated as a function of frequency. Such rotation can be realised by reflecting the squeezed light from *filter cavities* – long-storage-time optical cavities, operated in a detuned configuration, whose linewidth is comparable to the frequency range over which the squeezed quadrature must be rotated ($\sim$50 Hz) [9]. A recent investigation, using realistic parameters and noise estimates, concluded that a two-mirror cavity with an optical loss of 1 ppm/m would be sufficient to realise an effective filter cavity for an Advanced-LIGO-like interferometer [11].

Our measurements show that a confocal cavity approximately 10-20 m in length fulfils this requirement. Such a cavity can be constructed within the existing vacuum envelope of the LIGO interferometers without resorting to use of the long arm cavities. Frequency dependent squeezing is thus an attractive and viable near-term upgrade for Advanced LIGO.

Optical loss in long-storage-time cavities is a key parameter across a wide variety of disciplines. Our results demonstrate that, using currently available optics, 10 m-scale cavities with storage times of order 10 ms are now within reach.

Acknowledgements

The authors gratefully acknowledge the support of the National Science Foundation and the LIGO Laboratory, operating under cooperative Agreement No. PHY-0757058. They also acknowledge the guidance and invaluable input of Peter Fritschel and Nergis Mavalvala and fruitful discussion and collaboration with Josh Smith, Valery Frolov, Hiroaki Yamamoto and Jan Harms. Mirror transmissivity measurements were made possible through the assistance and expertise of Eric Gustafson and Liyuan Zhang. Myron MacInnis assisted in construction and maintenance of the experimental apparatus. This paper has been assigned LIGO Document No. ligo-p1300159.